Turbulent Patch Identification in Microstructure Profiles: A Method Based on Wavelet Denoising and Thorpe Displacement Analysis

JAUME PIERA

Department of Signal Theory and Communications, Universitat Politècnica de Catalunya, Barcelona, and Environmental Physics Group, Department of Physics, Universitat de Girona, Girona, and Department of Ecology, Universitat de Barcelona, Barcelona, Spain

ELENA ROGET

Environmental Physics Group, Department of Physics, Universitat de Girona, Girona, Spain

JORDI CATALAN

Department of Ecology, Universitat de Barcelona, Barcelona, and Centre d'Estudis Avançats de Blanes, CSIC, Girona, Spain

ABSTRACT

A new method based on wavelet denoising and the analysis of Thorpe displacements d_T profiles is presented for turbulent patch identification. Thorpe profiles are computed by comparing the observed density profile $\rho(z)$ and the monotonic density profile $\rho_m(z)$, which is constructed by reordering $\rho(z)$ to make it gravitationally stable. This method is decomposed in two main algorithms. The first, based on a wavelet denoising procedure, reduces most of the noise present in the measured profiles. This algorithm has been tested from theoretical profiles and has demonstrated a high efficiency in noise reduction, only some limitations were detected in very low-density gradient conditions. The second algorithm is based on a semiquantitative analysis of the Thorpe displacements. By comparing each displacement d_T with its potential error E_{dT}, it is possible to classify samples in three possible states: Z ($d_T = 0$), U ($d_T < E_{dT}$), and S ($d_T > E_{dT}$). This classification makes it possible to compute two statistical indexes: the displacement index I_D, the quotient between the number of S values and the number of averaging points; and the uncertainty index I_U, the quotient between the number of points on state U and the number of averaging points. The displacement index I_D has been used as the parameter for turbulent patch identification, identifying the patches as segments with strict positive I_D values. To illustrate the method, a number of field profiles covering a wide density gradient range were analyzed. Turbulent patches were validated following the tests proposed by Moum and Galbraith and Kelley. The high percentage of validating patches indicates that the proposed method is very efficient even at very low-density gradients where the potential error on d_T is high, and shows that it is a powerful tool for turbulent patch identification.

1. Introduction

One of the objectives of analyzing microstructure density profiles is to identify turbulent patches and computing its characteristic vertical length L_p. The characterization of the turbulent patches has usually been applied at depths with high-density gradients. The main reason for selecting high-density gradients is that diapycnal fluxes in the aquatic environments are mainly originated by turbulent mixing; therefore, realistic estimates of coefficients of vertical turbulent exchange must be based on the occurrence and properties of turbulence patches (Prandke and Stips 1992). In addition,

there is also a secondary operational reason: high-density gradients avoid the methodological constraints related to instrumental noise (Gregg 1987; Moum 1996a).

In recent years, the interest in relating turbulent mixing to biological processes has increased (see the special issue of *Scientia Marina,* 1997, vol. 61, suppl. 1). For example, the differences in turbulent regimes can yield vertical differences in population dynamics and selective processes among planktonic algae (Reynolds 1992), or zooplankton distribution (Haury et al. 1990). The changes in turbulent mixing regimes can be considered not only one of the main driving forces in the succession of the planktonic communities (Margalef 1983) but also a physical constraint for plankton evolution (Catalan 1999). To understand the relationship between the turbulent regimes and biological processes, turbulence must be characterized in a wider range of density gradients, starting from the low-density gradients typical

Corresponding author address: Dr. Jaume Piera, Department of Ecology, Universitat de Barcelona, Diagonal 645, Barcelona 08028, Spain.
E-mail: jpiera@porthos.bio.ub.es

in boundary layers to the high-density gradients characteristic of pycnoclines. Expanding turbulent patch characterization to low-density gradients can also be useful in many physical studies. The characteristics of turbulent patches near surface layers, where the density gradient is usually low, can provide valuable information to understand the exchange of momentum, heat, and mass between the atmosphere and natural water bodies.

Methods of turbulent patch identification: A brief review

Several algorithms and tests based on density profiles (or associated scalars, i.e., salinity or temperature) have been proposed for the identification of turbulent patches. These algorithms are usually derived from Thorpe's method (Thorpe 1977), which computes a reference density profile $\rho_m(z)$ by sorting the original density profile $\rho(z)$. Two distinct values can be computed from these density profiles: the density fluctuation, defined as $\rho'(z) = \rho(z) - \rho_m(z)$; and a Thorpe displacement $d_T(z)$. The latter is the vertical distance that an individual fluid particle (i.e., a single density value) of the original profile $\rho(z)$ has to be moved in order to generate the stable density profile $\rho_m(z)$.

Density fluctuations can be used to obtain quantitative information of the energetics of mixing by computing the available potential energy of the fluctuations (APEF; Dillon 1984):

$$\text{APEF} = \frac{g}{n\rho_0} \sum_{i=1}^{n} z_i \rho_i', \qquad (1)$$

where n is the number of samples associated to the patch, g is the acceleration of gravity, and ρ_0 is the average water density.

However, in the research of biological and physical interactions at small scale, Thorpe displacements may provide some quantitative information that cannot be achieved directly with density fluctuations. The estimation of water displacements may be required, for example, when relating turbulent mixing with the changes on the encounter rate between predator and prey, or the changes of the environmental light for photosynthetic organisms. The information derived from the displacements can be especially important in very low-density gradients, in which the small density fluctuations (that represent a very small variation on the available potential energy) can be associated to large vertical displacements.

Statistical properties of $\rho'(z)$ or $d_T(z)$ profiles are usually the main input for the algorithms of turbulent patch identification. To date, there is no accepted statistical model of overturning that can be used as a reference for validating the computed density fluctuation or Thorpe displacement profiles. The lack of any theoretical model has led to the search for methods for turbulent

patch identification based on heuristic reasoning and empirical parameters.

Dillon (1982) defined a complete overturn (i.e., a mixing patch) as the region where no heavier or lighter fluid particles in $\rho(z)$ relative to $\rho_m(z)$ are found outside the patch, and no heavier or lighter fluid particles relative to $\rho_m(z)$ outside the patch are found within it. The method relies on the ability to resolve density fluctuations on scales much smaller than the typical particle displacement necessary to create the reordered profile. Instrumental noise or mismatches in time response of temperature and conductivity probes may yield patterns of scales similar to mixing motions, especially at low-density gradients. Therefore, care should be taken when applying this method to weakly stratified environments, because the thickness of a turbulent patch can be greatly overestimated.

Gregg (1980) proposed zero-crossing counting as an alternative method of turbulent patch identification. In this method, a turbulent patch is identified as the depth interval at which the distance between consecutive zero-crossing density fluctuations are smaller than a certain threshold. To avoid potential artifacts caused by instrumental noise, only strongly pronounced patches (which imply a relative high background density gradient) are usually considered (Prandke and Stips 1992).

Moum (1996a,b) proposed two conditions to validate a turbulent patch. 1) Patches should contain only data with significantly different fluctuation signals from their respective noise levels; 2) patches must have well-defined upper and lower boundaries that yield two specific requirements: $L_{T\max} < L_p$, where $L_{T\max}$ denotes the maximum Thorpe displacement throughout the patch; and $\int d_T(z) \, dz$ over the depth range of the patch should be equal to 0. The first condition requires a relatively high stratification background level in order to obtain high values of fluctuation.

Galbraith and Kelley (1996) proposed an alternative test, which was initially developed for conductivity–temperature–depth (CTD) profiles, but it can also be used with microstructure data. The test is implemented in two parts. The first part of the test is focused on the artifacts derived from random noise. Density fluctuations are examined for "runs" of adjacent positive or negative values, defining the run length as the number of samples contained in each run. The probability density function (PDF) of the run length is compared with the PDF expected from random noise series. As a diagnostic parameter, the authors chose the root-mean square (rms) of the run lengths computed within a patch. This value decreased when the amount of random uncorrelated noise added to the observed profile was increased. This yields a threshold value for rms run length within an individual turbulent patch that must be exceeded in order for it to be validated. Patches with rms run length below the threshold are considered artifacts generated from random noise. The second part of the test rejects artifacts derived from systematic errors such

as salinity spikes, which are caused by time-response mismatches in temperature and conductivity sensors. Temperature and salinity covariations with respect to density are screened within the turbulent patch, and only patches with tight relationships between ρ, T, and S are validated. Calibration with examples from coastal and deep-sea environments indicates that this test can be used to validate turbulent patches in strongly stratified environments, but that noise will prevent the validation in weakly stratified environments.

The common feature of all the methods listed above is a general inability in identifying turbulent patches at low-density gradients. Here we proposed a new method that significantly improves patch detection at low-density gradients. The method is designed to reject patches caused by random noise, although it does not replace the need for careful data acquisition practices and for postprocessing to minimize the effects of systematic errors such as salinity spiking.

2. Proposed procedure for turbulent patch detection

a. Constraints on turbulent patch identification

Instrumental limitations derived from resolution and noise imposes basic constraints on turbulent patch detection. Assuming that turbulent patches can be identified from non-null values of Thorpe displacements, the limit for patch identification resides in the capacity to distinguish between displacements caused by instrument noise and those generated by turbulent processes.

It is not necessary to know the numerical value of d_T for displacement validation, only two conditions are required: 1) the displacements are different than 0, and 2) the error associated with each displacement E_{dT} is smaller than the displacement itself.

In order to evaluate E_{dT}, an error analysis based on the solid-body rotation model has been developed (Itsweire et al., 1986; Imberger and Boashash 1986) in which a cylindrical overturning eddy in a linear density profile yields a z-shaped $\rho(z)$ segment. In this model it is possible to express the length of the theoretical displacement d_T as a function of the stable density gradient $\partial\rho/\partial z$ (i.e., the local gradient computed from the monotonic profile), and the magnitude of the density fluctuation ρ':

$$d_T \approx \frac{\rho'}{\partial\rho/\partial z}. \qquad (2)$$

From (2) is possible to derive the relative error of d_T as

$$\frac{E_{dT}}{d_T} \approx \frac{E_{\rho'}}{\rho'} + \frac{E_{\partial\rho/\partial z}}{\partial\rho/\partial z}. \qquad (3)$$

Since the computation of local density gradient is based on a greater number of measurements than that of density fluctuation, we can neglect the contribution of the relative error of the monotonic density gradient. Then, from (2) and (3)

$$E_{dT} \approx \frac{E_{\rho'}}{\partial\rho/\partial z}. \qquad (4)$$

The error of Thorpe displacements E_{dT} is derived as a function of two parameters: the density gradient $\partial\rho/\partial z$ (which is imposed as a background condition), and the error on density fluctuation $E_{\rho'}$. Improving turbulent patch detection requires minimizing E_{dT}, which is only possible by reducing $E_{\rho'}$. In this case it is necessary to find a method for optimal density recovery that minimizes noise from the density profile without losing small density perturbations derived from the overturn motions at low-density gradients.

b. A wavelet analysis approach to noise reduction

In the last few years there has been considerable interest in the use of wavelet transforms for removing noise from data. When data are intermittent in nature, as is the case of density fluctuations, wavelet analysis is highly advantageous over either Fourier or real-space analysis (Pen 1999).

The wavelet transform of a function $f(x)$ with finite energy is defined as the integral transform with a family of functions $\Psi_{\lambda,\tau}(u) \equiv \lambda^{-1/2}\Psi[(u - \tau)/\lambda]$ and is expressed as

$$Wf(\lambda, \tau) = \int_{-\infty}^{\infty} f(u)\Psi_{\lambda,\tau}(u)\, du$$

$$= \int_{-\infty}^{\infty} f(u)\frac{1}{\sqrt{\lambda}}\Psi\left(\frac{u - \tau}{\lambda}\right) du, \qquad (5)$$

where λ is a scale parameter, τ a location parameter, and $\Psi_{\lambda,\tau}(u)$ are called wavelets. In the continuous wavelet transform (CWT) the wavelet transform can be computed for every value of λ and τ. For empirical measurements, discrete wavelet transform (DWT) is preferable since $f(x)$ is known at discrete points ($x = n_j$). This requires the discretization of (5) in the scale and space domain. The discretization of the domain of (5) is not arbitrary since it is necessary to conserve the amount of information in the signal. The simplest and most efficient case for practical computation is the dyadic arrangement (Daubechies 1992; Mallat 1989), where $\lambda = 2^m$ and $\tau = j2^m$ resulting in

$$\text{DWT}f(m, j) = \sum_{n=-\infty}^{\infty} f(n)\Psi_{m,j}(n)$$

$$= \sum_{n=-\infty}^{\infty} f(n)\frac{1}{\sqrt{2^m}}\Psi\left(\frac{n - j2^m}{2^m}\right). \qquad (6)$$

Mallat (1989) produced a fast wavelet (FWT) algorithm that computes the DWT very efficiently. The Mallat algorithm is a classical scheme in signal processing
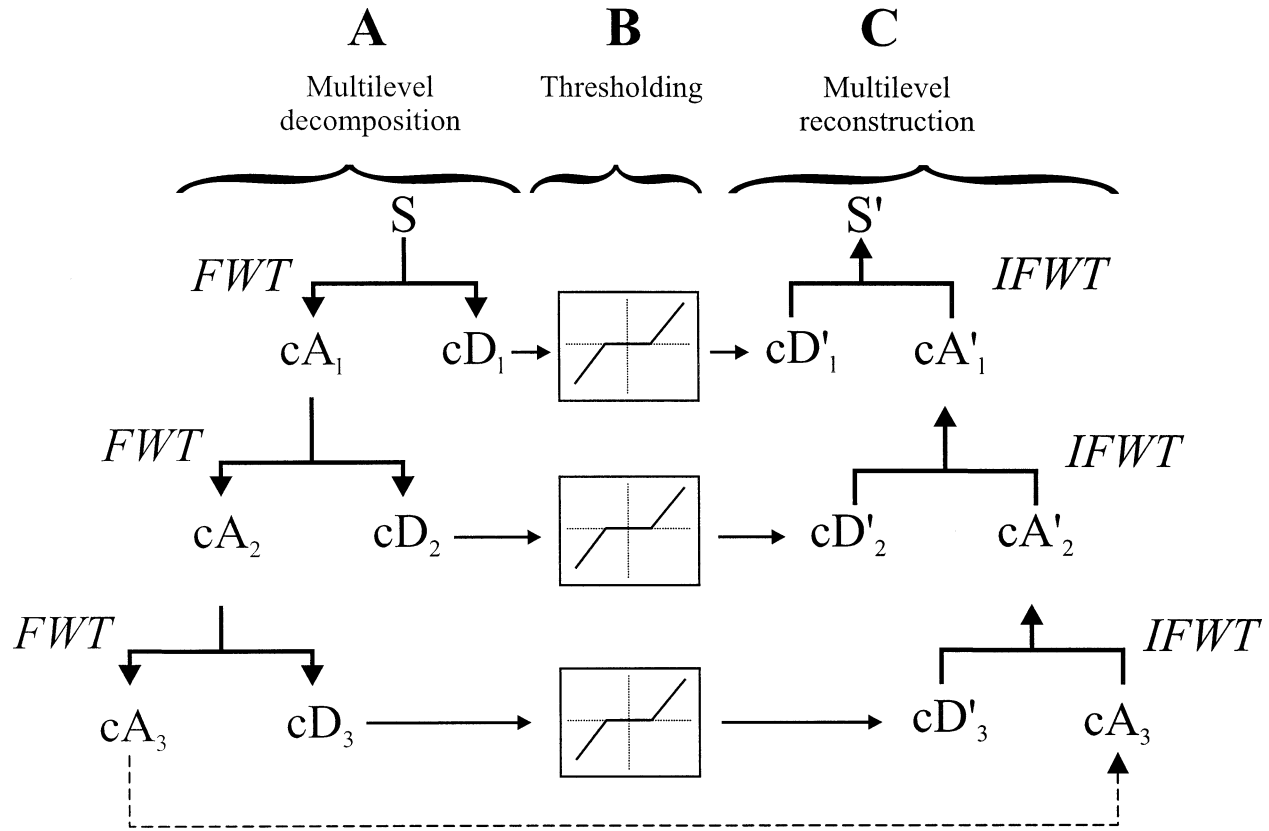
FIG. 1. Schematic diagram of the three steps of the denoising method: multilevel decomposition, thresholding, and multilevel reconstruction.

known as a two-channel subband coder using quadrature mirror filters (QMFs). The original signal is first decomposed into low- and high-frequency components by the convolution-subsampling operations with the pair consisting of a "low-pass" filter and a "high-pass" filter directly on the discrete domain. The low-frequency components (approximation coefficients) keep the global features of the signal, and the high-frequency components (detail coefficients) retain the local features. The decomposition process can be iterated recursively on the approximation coefficients while the detail coefficients are maintained intact. At the last iteration, both approximation and detail coefficients are kept. By applying such decomposition to the measured data (Cohen et al. 1993), it is possible to obtain empirical wavelet coefficients associated to different levels of local characterization.

The method for noise reduction here proposed is derived from a wavelet-thresholding algorithm based on Mallat's scheme (Donoho and Johnstone 1994; Donoho 1995), and it comprises three main steps (Fig. 1).

- *Multilevel decomposition*: FWT (Mallat 1989) is applied to decompose the signal into different levels of local characterization. Figure 1a shows an example of this hierarchical decomposition. In this example, the level of decomposition was set to 3, yielding one series of approximation coefficients cA_3 and a set of three distinct detail coefficient signals $cD_{1,2,3}$.

- *Thresholding*: The method assumes that the noise can be modeled as a random Gaussian signal, so the major part of the noise is finally stored in the detail coefficients. To reduce noise contribution, a threshold function is applied to the detail coefficients, thereby suppressing those coefficients smaller than certain amplitude (Fig. 1b).

- *Multilevel reconstruction*: A denoised profile can be recovered from the transformed coefficients by applying the inverse fast wavelet transform (IFWT) recursively over each level of decomposition (Fig. 1c).

One of the most important advantages of this method is that it not only optimizes the mean-square error but also ensures, with high probability, that the denoised signal is at least as smooth as the original (Donoho 1995). Alternative techniques that simply optimize the mean-square differences can, in some cases, generate undesirable noise-induced structures ("ripples," "blips," and oscillations), which may generate interpretative artifacts on density fluctuations and Thorpe displacements. An example of the advantages of the multiscale approach of this method on measured data is shown in Fig. 2. Unlike the classic low-pass-filtering applications, it is possible to smooth the segments where
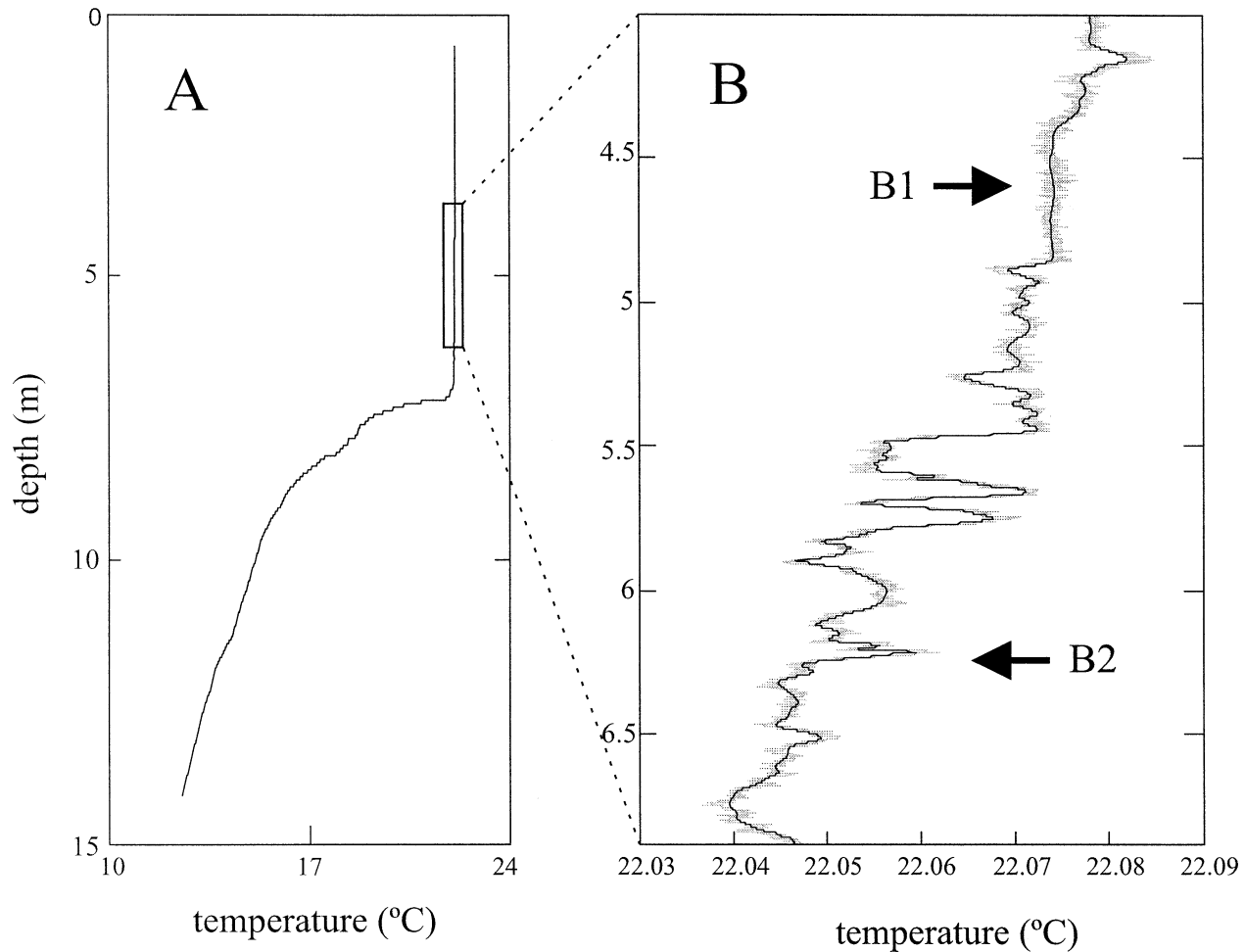
FIG. 2. (a) Example of the denoising method applied to a real temperature profile. (b) The detail of the profile shows that the method smoothens the segments in which there are no significant changes (B1) but keeps the small fluctuations appearing at low-density gradients (B2).

there are no significant changes [Fig. 2b(B1)] while keeping the small fluctuations appearing at low-density gradients [Fig. 2b(B2)].

NOISE SENSITIVITY ANALYSIS: THEORETICAL TEST

With no accepted statistical model of overturning, there is little guidance to confirm from field data whether

TABLE 1. Features of the five segments of the theoretical profile used for testing the numerical limitations of the denoising method.

Segments			Overturns	
	Interval			
Number	depth (m)	N^2 (s^{-2})	Depth (m)	Size (m)
1	0.00–1.50	6.25×10^{-6}	0.75	0.2
2	1.50–2.00	4.00×10^{-6}	1.75	0.2
3	2.00–2.75	2.25×10^{-6}	2.35	0.2
4	2.75–4.25	1.00×10^{-6}	3.50	0.3
5	4.25–7.25	2.50×10^{-7}	5.00	0.4
			6.50	0.3

density fluctuations are caused by overturning motions or whether they are artifacts from instrumental noise or numerical postprocessing. For this reason a set of theoretical profiles were designed for quantifying the potential error of d_T in the proposed denoising method. These profiles were based on the solid-body rotation model. Although this model is an oversimplification of real structures, it is easy to check the error contribution by comparing the theoretical z-shaped structures with the final result. It is not possible to guarantee the optimal recovering on real data with this test, but it does give some clues about the limitations of the numerical method. To determine the resolution limits for patch detection, the test was designed using the worst field conditions, namely, low buoyancy frequencies and small overturn sizes. The first test profile comprises five segments, each with a different associated buoyancy frequency. Hypothetical overturns were simulated in each segment. In the fifth segment (the most critical), two overturns of different length were simulated. A complete description is given in Table 1.
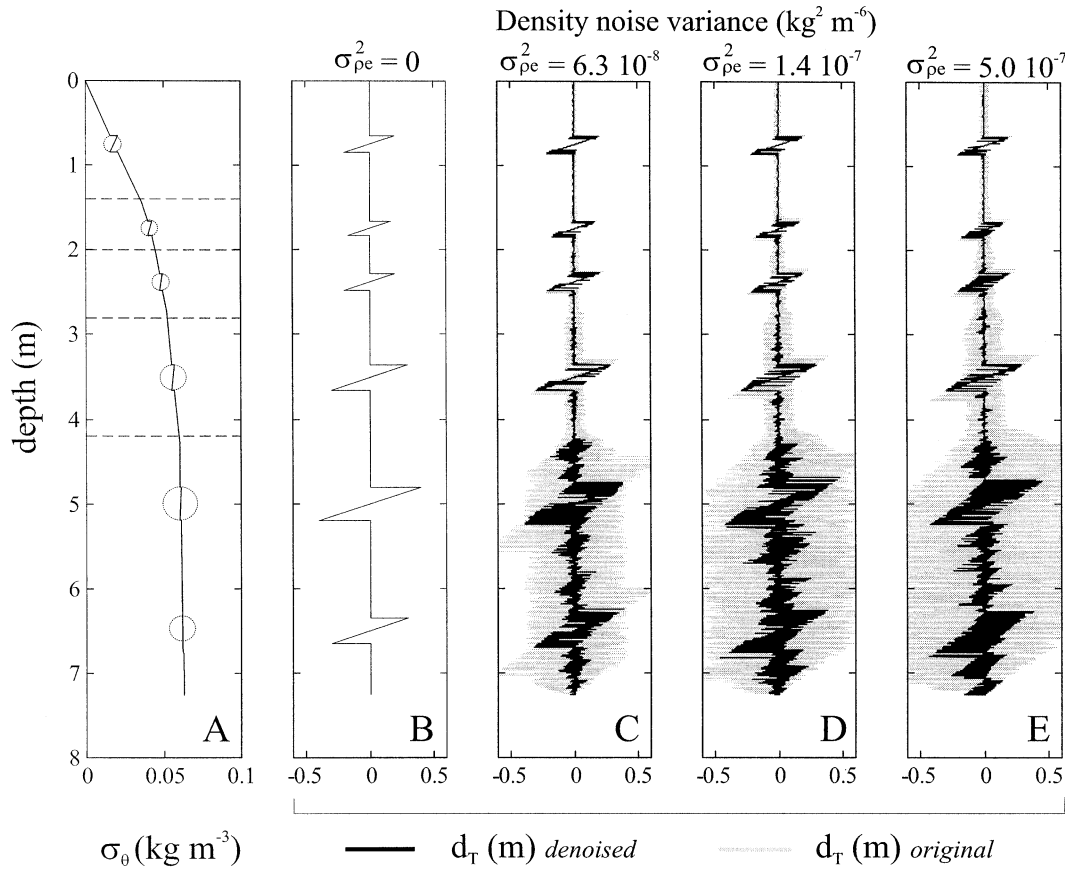
Density noise variance (kg^2 m^{-6})

FIG. 3. Noise sensitivity test applied to d_T computation. (a) Theoretical density profile used for the test. The circles indicate the depth and size of the theoretical overturns. (b) The d_T profile computed from (a). (c)–(e) The d_T profiles computed from (a) adding increasing levels of noise N_σ. The d_T profiles obtained with (black) and without (gray) applying the denoising method. See text for further details.

The other theoretical profiles were constructed by adding increasing levels of zero mean Gaussian white noise to the initial profile. The noise level for the first noisy profile was derived from the density error variance equation due to electronic and quantification error proposed by Gregg (1979):

$$
\begin{aligned}
\sigma_{\rho e}^2 &= \sigma_T^2 \left(\frac{\partial \rho}{\partial T}\right)^2 + \sigma_P^2 \left(\frac{\partial \rho}{\partial P}\right)^2 + \sigma_S^2 \left(\frac{\partial \rho}{\partial S}\right)^2 \\
&= \sigma_T^2 \left[\left(\frac{\partial \rho}{\partial T}\right)^2 + \left(\frac{\partial S}{\partial T}\right)^2 \left(\frac{\partial \rho}{\partial S}\right)^2\right] \\
&\quad + \sigma_P^2 \left[\left(\frac{\partial \rho}{\partial P}\right)^2 + \left(\frac{\partial S}{\partial P}\right)^2 \left(\frac{\partial \rho}{\partial S}\right)^2\right] \\
&\quad + \sigma_C^2 \left(\frac{\partial S}{\partial C}\right)^2 \left(\frac{\partial \rho}{\partial S}\right)^2,
\end{aligned}
\tag{7}
$$

where ρ is density; S salinity; T temperature; C is conductivity; and σ_S^2, σ_T^2, σ_C^2, σ_P^2 are the noise variance of

salinity, temperature, conductivity, and pressure, respectively.

Based on laboratory test measurements of the microstructure sensors and considering the worst case for the partial derivatives in (7) the estimated density error variance, $\sigma_{\rho e}^2$, was 6.25×10^{-8} kg^2 m^{-6}. To consider added uncertainties in field measurements, a factor of 50% and 100% increase in noise was also computed, yielding two new density profiles with noise variance $\sigma_{\rho e}^2$ of 1.40×10^{-7} and 5×10^{-7} kg^2 m^{-6}, respectively.

The test was developed in two steps. First, the denoising method was applied over the noisy theoretical density profiles. The multilevel wavelet transform was based on Daubechies wavelet (Daubechies 1992) and the level of decomposition was set to 9.

Detail coefficients were transformed by applying a soft threshold function (Donoho 1995):

$$
cD' = \begin{cases} \text{sgn}(cD)|cD - \text{thr}| & cD > \text{thr} \\ 0 & cD < \text{thr}. \end{cases}
\tag{8}
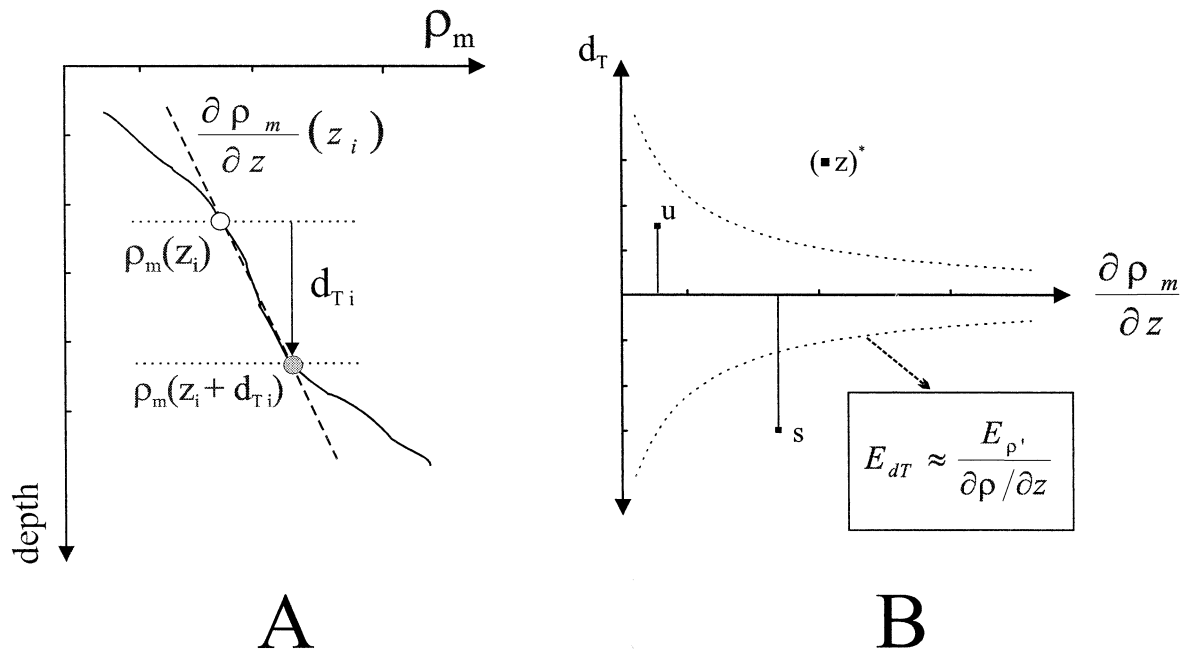$$

With this function, coefficients smaller than the

FIG. 4. Diagram of the of local gradient classification method. (a) Scheme of the local density gradient computation. (b) Comparing displacement values with their potential error allows the classification of each displacement into one of the following categories: Zero (Z), Uncertain (U), and Signal (S).

threshold "thr" are suppressed while the rest of the coefficients are shrunk an equivalent of the threshold value. The threshold value was selected as in Donoho and Johnstone (1994):

$$\text{thr} = \xi \sqrt{2 \, \log(n)}, \qquad (9)$$

where n is the number of samples and ξ is a rescaling factor estimated from the noise level present in the signal. The estimation of the noise level was based on first level of detail coefficients cD_1 well suited for zero mean Gaussian white noise in the denoising 1D model (Misiti et al. 1996):

$$\xi = \frac{\text{median}(|cD_1|)}{0.6745}. \qquad (10)$$

Once the synthetic density profiles were denoised, the Thorpe displacements were computed by comparing the result calculated from the original theoretical profile (without noise) to the Thorpe displacements calculated from the denoised density profiles.

Figure 3 shows the graphical results of this test. By comparing the denoised results (Figs. 3c–3e) with the expected profile (Fig. 3b), overturns were clearly resolved in the first four segments. In the last segment, which is the most critical because it has the lowest density gradient, noise was reduced considerably, but its effects yielded a significant error in the estimation of displacements and some spurious overturns appeared.

c. Local gradient classification method for patch identification

To overcome the artifacts generated from the remaining noise, a complementary method based on a semiquantitative analysis of d_T was implemented.

The method compared the displacement d_T and its error E_{dT}. The error E_{dT} was computed from (4). The error on density fluctuation $E_{\rho'}$ was estimated as the standard deviation of noise $\sigma_{\rho e}$ according to (7). Instrumental errors were estimated based in Luketina (1986). The local density gradient $\partial \rho / \partial z$ (which can change significantly depending on the scale considered) was computed over the depth range defined by the depth of the particle in the original profile and the depth associated with the monotonic profile (Fig. 4a).

Comparisons of the displacement and its potential error were categorized into three possible states (Fig. 4b). The sample was labeled Zero (Z) when it had the same associated depth in the original and the monotonic density profiles (i.e., $d_T = 0$). The label Uncertain (U) was assigned when Thorpe displacement was smaller than the associated error. Finally, the label Signal (S) was assigned when the value of the displacement was larger than the associated error. In this case it was possible to ensure that the sample has non-null Thorpe displacement.

Two statistical indexes that consider the percentage of each data category in a depth range were defined. The displacement index (I_D) was computed as the quotient between the number of S values and the number
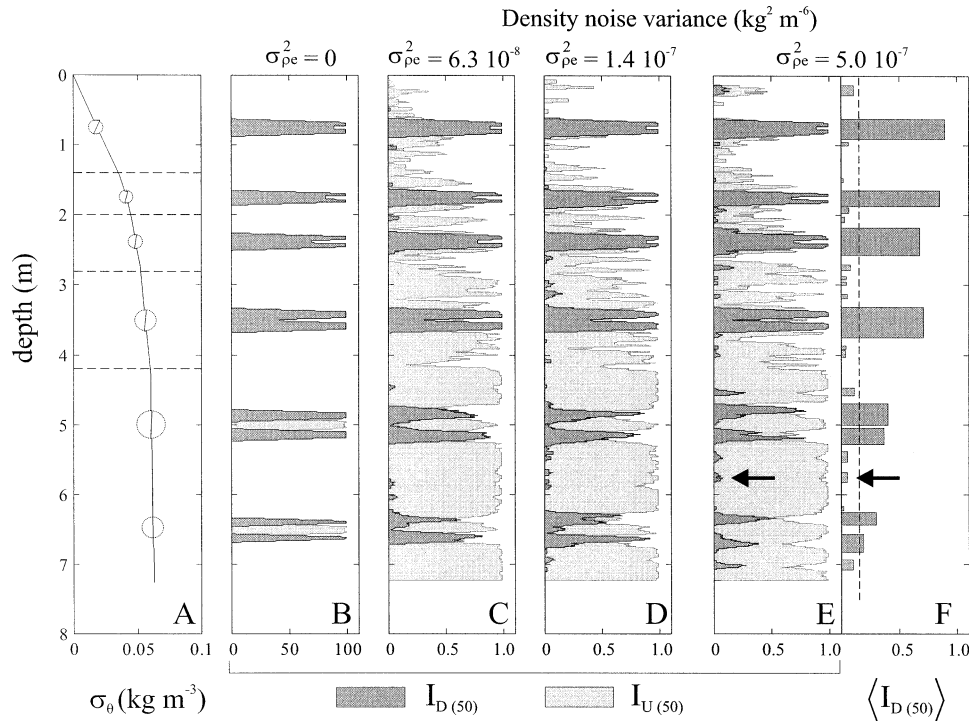
FIG. 5. Noise sensitivity test applied to I_D index computation (in dark gray). (a) Theoretical density profile used for the test. Circles indicate the depth and size of the theoretical overturns. (b) Displacement index I_D in dark-gray and uncertainty index I_U in light-gray computed from (a). (c)–(e) The I_D and I_U computed from (a) with increasing levels of noise added $\sigma_{\rho e}^2$. (f) Mean displacement index computed from every patch detected in (e), a threshold $thres_{\langle ID(50) \rangle} = 0.1$ has been represented (in dotted line) showing that all the false turbulent patches are below this value. See text for further details.

of averaging points. It indicates the percentage of samples that unambiguously have displacements different from zero. The uncertainty index I_U was computed as the quotient between the number of points on state U and the number of averaging points. It provides an estimation of the measurement uncertainty.

The displacement index I_D was used for turbulent patch identification. Segments with I_D equal to zero were assumed to delimit the turbulent patches, and thus turbulent patches were identified as segments with strict positive I_D values. With this method, the size of the turbulent patches may be overestimated depending on the number of samples considered for computing the displacement index. The incremented size can be estimated as $2n\Delta z$, where n is the number of averaged samples and Δz is the spatial resolution of the measurements. Considering a 1-mm spatial resolution (a com-

mon value in microstructure profiles) and $n = 50$, the overestimation would be 10 cm, which can be neglected in big patches, but it can represent a significant increase when the patches are small. In order to overcome the potential artifact, the vertical size of the patches was reduced by decreasing their vertical boundaries (z_init, z_end) an equivalent of $n\Delta z$ (i.e., the new boundaries were computed as ($z\_init + n\Delta z$, $z\_end - n\Delta z$), depth positive downward).

NOISE SENSITIVITY ANALYSIS: THEORETICAL TEST

Following the same approach as that of the denoising procedure test, the set of theoretical profiles with different noise levels was used to evaluate the limits of the method (Fig. 4). The values of I_D and I_U were computed over 50 samples, which is a reasonable number for statistical robustness and spatial resolution (50 samples correspond approximately to 5 cm for spatial resolution of 1 mm). Figure 5 shows the results of the indexes computed from the sensitivity test profiles. The I_D values are represented as solid dark gray areas, while I_U values are in light gray. The theoretical I_D profile (Fig. 5b) shows how turbulent patches can be delimited as segments of strict positive I_D values, although in the fifth segment, each overturn was split in two separate

TABLE 2. Characteristics of the reservoirs and lake from where the field data surveys were conducted.

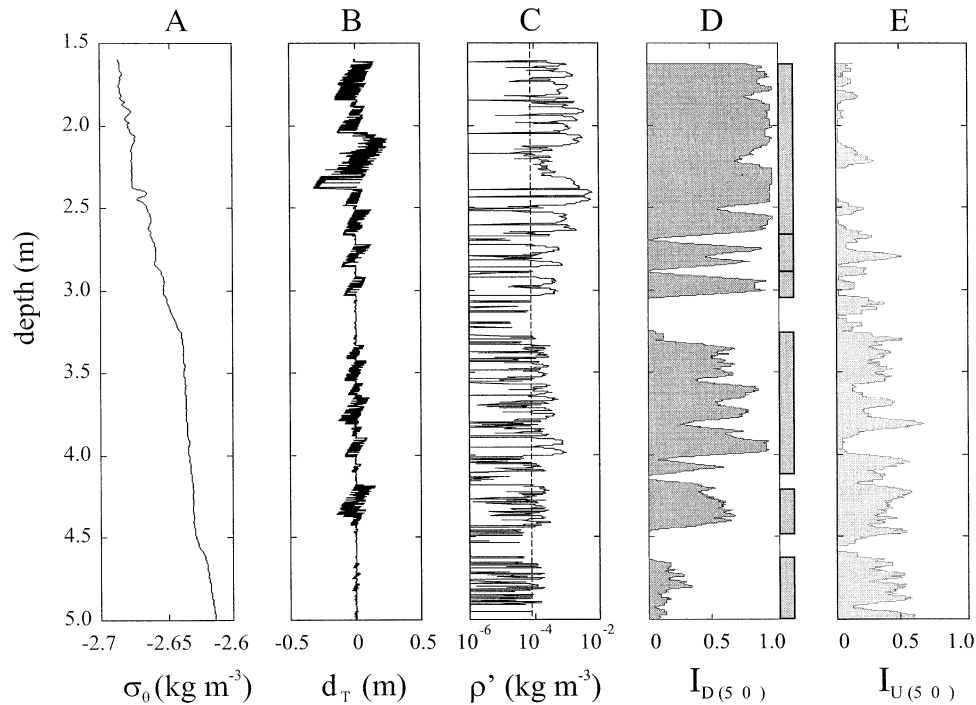| Location	Profiler	Depth mean (max) (m)	Total area (m²)	Volume (m³)
Boadella Reservoir	MST	17.0 (54.0)	3.6×10^6	62×10^6
Sau Reservoir	MP	26.3 (55.0)	5.8×10^6	124×10^6
Lake Banyoles	MST	15.7 (45.0)	1.1×10^6	17×10^6

FIG. 6. Example of I_D and I_U computation with field data, corresponding to one of the profiles obtained in the Lake Banyoles. (a) Potential density (dotted line indicates the estimated value for $E_{\rho'}$). (b) Thorpe displacement. (c) Density fluctuations. (d) The I_D index. Rectangles indicate the depth range of the patches identified. (e) The I_U index.

patches due to the low displacements in the central part of the overturns. The I_D profiles computed from the increasing noise profiles were solved in a very similar way, but several false patches of small size appeared (Figs. 5c–5e). However, even for the noisiest profile (Fig. 5e) it was possible to reject the false patches from the rest by computing the mean I_D (Fig. 5f). All the false turbulent patches were characterized by small values of $\langle I_D \rangle$. As an example, the mean value of the false patch seen in Fig. 5e was also seen in Fig. 5f. By computing the mean value for every patch it is possible to define a threshold of $\langle I_D \rangle$ to reject the false patches generated by noise. In this test the threshold was determined as $\text{thres}_{\langle ID(50) \rangle} = 0.1$ (dotted line in Fig. 5f).

The index I_U was computed to show how the level of uncertainty increases when some noise is added to the original profile. The high level of uncertainty explains why many algorithms fail to detect turbulent

patches at low-density gradients. However, our results suggest that I_D is a robust parameter for turbulent patch identification, as it is computed only from validated displacements.

3. Application to field data

Four series of microstructure profiles were used to test the proposed method. Data were obtained from sensors mounted on two distinct free-falling/rising microstructure profilers. The first probe was the MSS profiler, developed by ISW Wassermesstechnik and Sea&Sun Technology. The second was the MP profiler developed by the Centre for Water Research (CWR), which at present is commercialized, with an improved data acquisition system (Carter and Imberger 1986), by Precision Measurement Engineering as the Self Contained Autonomous Microprofiler (SCAMP). Both instruments

TABLE 3. Results of the turbulent patches obtained from the series of profilers. The first column indicates the depth range considered in each series. The buoyancy frequency computed from the range depth has been included showing the differences in background density gradient. Patches were rejected when the mean I_D was below the threshold [$\text{thres}_{\langle ID(50) \rangle} = 0.1$].

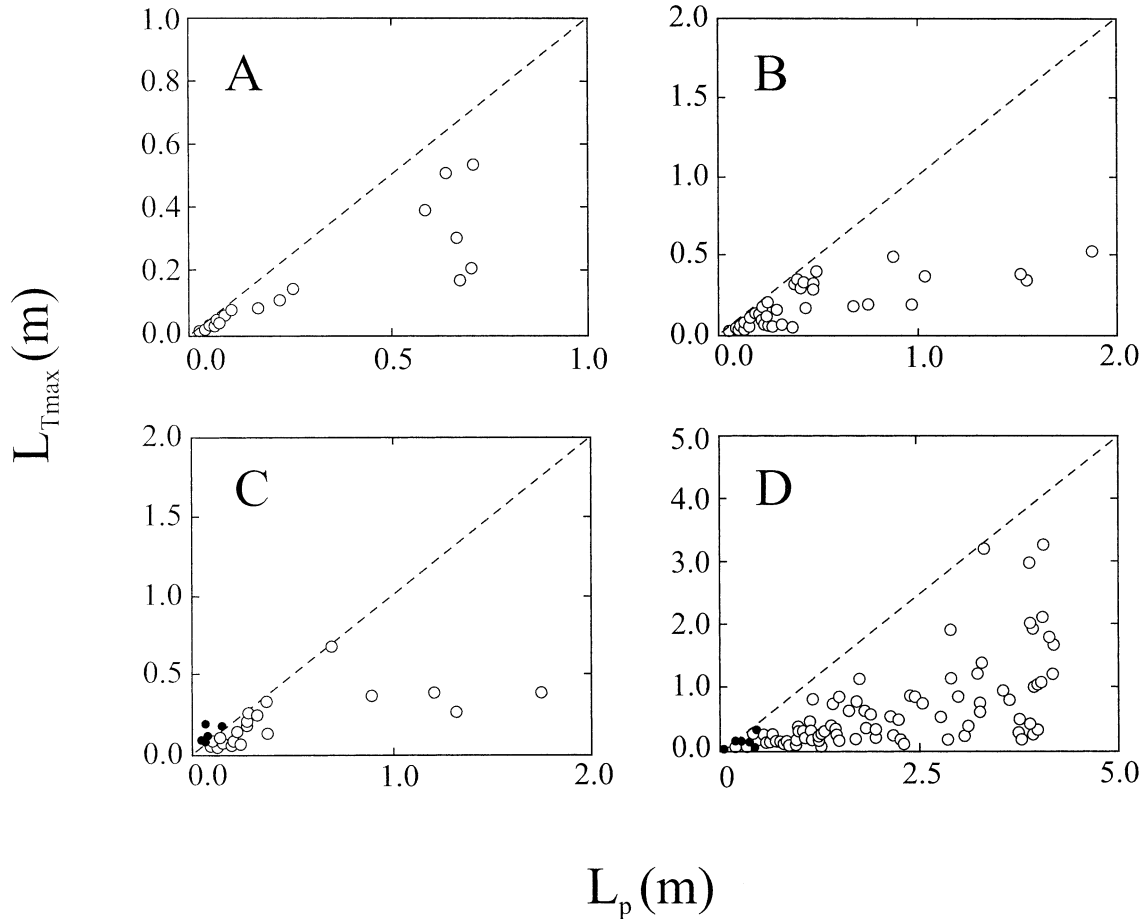| Ref.	Location	Depth range (m)	N^2 (s^{-2})	Total profiles	Patch detected	Patch rejected
A	Boadella	7.0–9.0	$(1.25–2.02) \times 10^{-4}$	27	41	5
B	Banyoles	7.0–9.0	$(4.99–13.93) \times 10^{-5}$	83	90	3
C	Sau	10.0–16.0	$(2.59–5.73) \times 10^{-5}$	42	46	8
D	Banyoles	0.0–4.5	$(1.08–10.56) \times 10^{-6}$	83	181	9

FIG. 7. Patch length L_p vs maximum Thorpe displacement within the patch $L_{T\max}$. The plots correspond to the different series of field measurements (referenced according to Table 3). Rejected turbulent patches according to Moum's (1996a,b) method are indicated as solid circles.

use a fast response thermistor FP07 (Thermometrics) for microstructure temperature measurements. The MP profiles were obtained by raising the profiler at nominal rate of 0.1 m s^{-1} and sampling data at 100 Hz, while MSS profiles were obtained by falling the profiler at nominal rate of 0.6 m s^{-1} and sampling data at 1024 Hz. In both cases, the spatial resolution was close to 1 sample per millimeter.

The profile series were obtained in three field surveys. In each series a fixed depth range was selected to illustrate a range of background density gradients. The surveys were performed at Sau reservoir, Boadella reservoir, and Lake Banyoles, situated north of Catalonia, Spain. Table 2 summarizes the morphometric features of these three freshwater bodies. In these systems the influence of salinity to density changes can be neglected because of its low values and insignificant gradients. Therefore, the main problem in detecting turbulent patches was exclusively derived from noise instrumentation in temperature measurements, avoiding problems from mismatches of the sensors in time response.

The profiles were processed following the method-

ology proposed. Denoised pressure profiles were obtained following the algorithm given in section 2. The temperature profiles were processed in two steps. First, temperature values were interpolated to regular depth intervals using the denoised pressure profile as the spatial reference. This step was necessary because the wavelet transform is based on regular sampled data. In the second step, the interpolated temperature profile was denoised following the proposed algorithm. Then, density was determined from denoised temperature, denoised pressure profiles, and salinity (derived from a fixed value of conductivity) following Chen and Millero (1986). Potential density was determined following Wüest et al. (1996). The background density gradient was evaluated in the range of selected depths by computing the buoyancy frequency $N^2 = (1/\rho_m)(\partial \rho_m/\partial z)$, where ρ_m was the monotonic density profile. Finally, turbulent patches were identified by applying the semiquantitative analysis of the Thorpe displacements, which were computed from the potential density profiles. The values of I_D and I_U were computed over 50 points, and the patches were identified as depth seg-
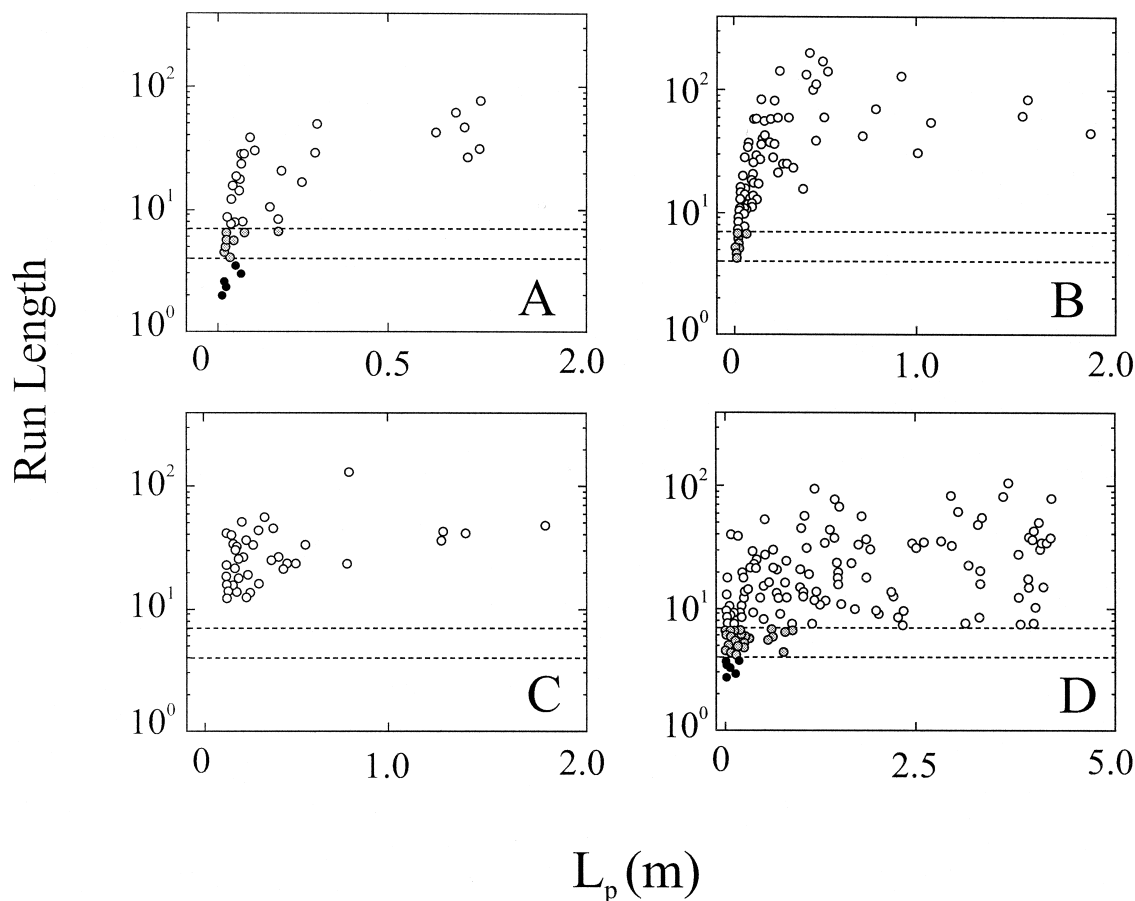
FIG. 8. Patch length L_p vs run length test, according to Galbraith and Kelley (1996). The plots correspond to the different series of field measurements (referenced according to Table 3). Rejected turbulent patches are indicated as black solid circles (threshold = 4) or gray solid circles (threshold = 7).

ments which had strictly positive $I_{D(50)}$ values. Figure 6 shows an example of the computed d_T, $I_{D(50)}$, and $I_{U(50)}$ profiles for one of the profiles obtained at Boadella reservoir. Table 3 summarizes the results for the profile series. The series has been tabulated from the highest $[N^2 = O(10^{-4})]$ to the lowest $[N^2 = O(10^{-6})]$ background density gradients.

A total of 358 patches were identified, but 25 were rejected considering that their mean I_Ds were below the threshold established (thres$_{\langle ID(50)\rangle}$ = 0.1). The final result yields a total of 333 turbulent patches identified.

The tests proposed by Galbraith and Kelley (1996) and Moum (1996a,b) were used for validating the turbulent patches identified from the displacement index $I_{D(50)}$. For these tests, it was necessary to compute three characteristic parameters of the turbulent patches: the vertical length L_p, the maximum Thorpe displacement throughout the patch $L_{T\max}$, and the rms value of run length of ρ'.

Moum's test validates the turbulent patch when $L_{T\max} < L_p$, and $\int d_T(z)\, dz$ over L_p is equal to 0. In order to consider the error in computing the Thorpe displace-

ment, the second condition was relaxed to $\int d_T(z)\, dz < 0.05\, L_p$.

Figure 7 shows the test validation results on the plots of patch length L_p and maximum Thorpe displacement $L_{T\max}$ associated to the turbulent patches detected. Those rejected are given as solid circles and all have a small patch length value. From the total of 333 identified patches with the method here proposed, 309 (92.8%) were validated according to Moum's test.

Galbraith and Kelley's (1996) run length test is based on run length series of density fluctuations. Patches with rms run length below the threshold are considered artifacts generated from random noise. The authors proposed a threshold of seven derived from CTD measurements and numeric simulations. However, in the case of microstructure profiles, it could be possible to reduce the threshold to four as first analyses indicates that patches with run lengths of four or more are statistically different from noise (P. S. Galbraith 2001, personal communication). As the threshold is derived empirically, guided by visual inspection of turbulent patches (Galbraith and Kelley 1996), the two threshold values

were considered in order to reflect the sensitivity and the robustness of the threshold selection.

Figure 8 shows the test validation results obtained from the four series of microstructure profiles (Table 3) according to the Galbraith and Kelley test. From the total 333 detected patches, 10 patches (3.0%) had a run length smaller than 4; 58 patches (17.4%) had a run length between 4 and 7; and 265 (79.6%) had a run length greater of 7. Even for the most restrictive threshold (7) and for the lowest-density gradient (Fig. 8d) the rejected patches correspond to the small size range.

4. Summary and conclusions

A new algorithm is presented based on a semiquantitative analysis of Thorpe displacement d_T and a wavelet-denoising algorithm to identify turbulent patches and computing its vertical scale L_p. Our results show that the denoising algorithm is very efficient in reducing noise level in the measured data, which is especially important for increasing the resolution of the patch identification method.

A set of theoretical profiles was designed for testing the limits of the denoising and patch identification methods. The results from this test show that it is possible to identify small patches even in the critical conditions of extreme low-density gradients. The final results obtained from different series of field data were validated following Moum's (1996a,b) test (92.8% of validated patches), and Galbraith and Kelley's (1996) test (97.0% of validated patches using a rms run length threshold of 4). This high percentage of validated patches shows the robustness of the method for detecting turbulent patches in a wide range of density gradients.

The main features of this new method are as follows. 1) *General applicability*: The method can detect the turbulent patches in very low-density gradients. This feature is especially important in the case of turbulent boundary layer characterization, where the gradient is usually low. It is also relevant in the studies of the interaction between turbulence and biological processes, because in these cases it is necessary to characterize the turbulent patches in a wide range of density gradients. 2) *Robustness*: The uncertainties derived from noise should not significantly change the final identification. The results obtained with the test demonstrate that the method is very robust, as the global features of the detected patches do not change with different noise levels.

APPENDIX

Pseudocode of the Proposed Method

1) Denoise raw depth.

   - Wavelet multilevel decomposition
   - Compute threshold and apply soft thresholding
   - Wavelet multilevel reconstruction

2) Interpolate raw temperature and conductivity to regular depth.
3) Denoise regular raw temperature and regular raw conductivity (as in step 1).
4) Compute density profiles from denoised temperature, conductivity, and depth.
5) Compute monotonic density profile.
6) Compute density fluctuations and Thorpe displacements.
7) Evaluate local density gradient from monotonic density and Thorpe displacement.
8) Compute $I_{D(50)}$ and $I_{U(50)}$ (window of 50 points, i.e., 0.05 m with 1-mm depth resolution).
9) Identify turbulent patches (consecutive samples with $I_{D(50)} > 0$).
10) Reduce the overestimated size of the turbulent patch derived from windowing effect (i.e., 0.05 m at each end).

REFERENCES

Carter, G. D., and J. Imberger, 1986: Vertically rising microstructure profiler. *J. Atmos. Oceanic Technol., 3,* 462–471.

Catalan, J., 1999: Small-scale hydrodynamics as a framework for plankton evolution. *Japan J. Limnol., 60,* 469–490.

Chen, C. T., and F. J. Millero, 1986: Precise thermodynamic properties for natural waters covering only the limnological range. *Limnol. Oceanogr., 31,* 657–662.

Cohen, A., I. Daubechies, B. Jawerth, and P. Vial, 1993: Multiresolution analysis, wavelets and fast wavelet transform on an interval. *Comptes Rendus Acad. Sci. Paris, 316A,* 417–421.

Daubechies, I., 1992: *Ten Lectures on Wavelets.* CBMS-NSF Regional Conference Series in Applied Mathematics, Vol. 61, Society for Industrial and Applied Mathematics, 357 pp.

Dillon, T. M., 1982: Vertical overturns: A comparison of Thorpe and Ozmidov length scales. *J. Geophys. Res., 87,* 9601–9613.

——, 1984: The energetics of overturning structures: Implications for the theory of fossil turbulence. *J. Phys. Oceanogr., 14,* 541–549.

Donoho, D. L., 1995: De-noising by soft-thresholding. *IEEE Trans. Inf. Theory, 41,* 613–627.

——, and I. M. Johnstone, 1994: Ideal spatial adaptation by wavelet shrinkage. *Biometrika, 81,* 425–455.

Galbraith, P. S., and D. E. Kelley, 1996: Identifying overturns in CTD profiles. *J. Atmos. Oceanic Technol., 13,* 688–702.

Gregg, M. C., 1979: The effects of bias error and system noise on parameters computed from *C, T, P,* and *V* profiles. *J. Phys. Oceanogr., 9,* 199–217.

——, 1980: Zero crossings of temperature microstructure. *Marine Turbulence,* J. C. J. Nihoul, Ed., Elsevier, 135–142.

——, 1987: Diapycnal mixing in the thermocline: A review. *J. Geophys. Res., 92,* 5249–5286.

Haury, L. R., H. Yamazaky, and E. C. Itsweire, 1990: Effects of

turbulent shear flow on zooplankton distribution. *Deep-Sea Res.,* **37,** 447–461.

Imberger, J., and B. Boashash, 1986: Application of the Wigner–Ville distribution to temperature gradient microscale: A new technique to study small-scale variations. *J. Phys. Oceanogr.,* **16,** 1997–2012.

Itsweire, E. C., K. N. Helland, and C. W. Van Atta, 1986: The evolution of grid-generated turbulence in a stably stratified fluid. *J. Fluid Mech.,* **162,** 299–338.

Luketina, D. A., 1986: Frontogenesis of freshwater overflows. Ph.D. dissertation, Center of Water Research, University of Western Australia, 200 pp.

Mallat, S., 1989: A theory for multiresolution signal decomposition: The wavelet representation. *IEEE Trans. Pattern Anal. Mach. Intell.,* **11,** 674–693.

Margalef, R., 1983: *Limnología.* Ediciones Omega, 1010 pp.

Misiti, M., Y. Misiti, G. Oppenheim, and J. M. Poggi, 1996: *Matlab Wavelet Toolbox User's Guide.* The MathWorks, Inc., 626 pp.

Moum, J. N., 1996a: Efficiency of mixing in the main thermocline. *J. Geophys. Res.,* **101,** 12 057–12 069.

——, 1996b: Energy-containing scales of turbulence in the ocean thermocline. *J. Geophys. Res.,* **101,** 14 095–14 109.

Pen, U. L., 1999: Application of wavelets to filtering of noisy data. *Philos. Trans. Roy. Soc. London,* **357A,** 2561–2571.

Prandke, H., and A. Stips, 1992: A model of Baltic thermocline turbulence patches, deduced from experimental investigations. *Cont. Shelf Res.,* **12,** 643–659.

Reynolds, C. S., 1992: Dynamics, selection and composition of phytoplankton in relation to vertical structure in lakes. *Arch. Hydrobiol. Beih. Ergeb. Limnol.,* **35,** 13–31.

Thorpe, S. A., 1977: Turbulence and mixing in a Scottish loch. *Philos. Trans. Roy. Soc. London,* **286A,** 125–181.

Wüest, A., G. Piepke, and J. D. Halfman, 1996: Combined effects of dissolved solids and temperature on the density stratification of Lake Malawi. *The Limnology, Climatology and Paleoclimatology of the East African Lakes,* T. C. Johnson and E. O. Oada, Eds., Gordon and Breach Scientific, 183–202.